Technische Universität München

^{41}Ca in interplanetary dust

Bachelor's Thesis

Stephan Jahn

July 2012

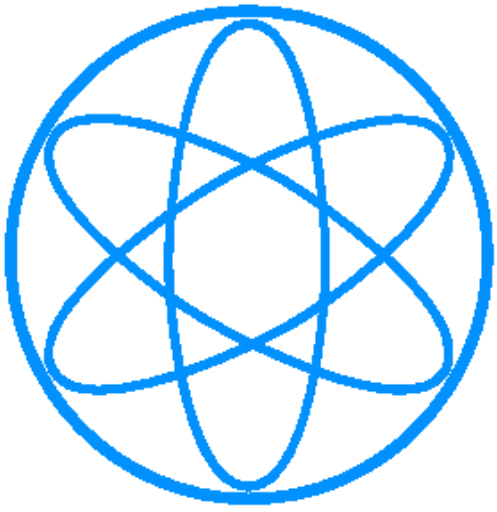

Physik Department

Summary

In this work, ^{41}Ca is discussed as tracer for interplanetary dust on earth for the first time. The annual influx of extraterrestrial ^{41}Ca has been calculated to lie between $1\frac{at}{cm^2\,yr}$ and $10^3\frac{at}{cm^2\,yr}$. Furthermore, it is shown that the extraterrestrial ^{41}Ca in Antarctica is measurable with the AMS-facility at the Maier-Leibnitz Laboratory in Garching. Antarctica is chosen as sampling site, because there is low influx of terrestrial dust. However, to distinguish between terrestrial and extraterrestrial produced ^{41}Ca more research about the terrestrial contribution has to be done.

Contents

Introduction

Between 20 and 60 thousand tons of micrometeorites are accreted on earth every year. Those micrometeorites have typical diameters of 200µm, so they are invisible to the naked eye. Nevertheless, most of the extraterrestrial matter comes to earth as such micrometeorites [1]. Characterising and tracing this micrometeoritic extraterrestrial matter is the challenge of this work. In order to do so, unique indicators capable to prove extraterrestrial origin have to be found. Long lived radionuclides are the most promising possibility. The idea is to test terrestrial samples for isotopes which are only, or at least overwhelmingly, produced extraterrestrial. For the first time, in this work ^{41}Ca is examined in the context of interplanetary dust. A similar approach is currently made with ^{53}Mn [2]. ^{53}Mn and ^{41}Ca are produced in the atmosphere only to an insignificant amount because there are only traces of appropriate target material. Lighter radionuclides (^{26}Al, ^{36}Cl) can for example be atmospherically produced by spallation of atmospheric ^{40}Ar (terrestrial background) [3]. For ^{41}Ca, one significant known terrestrial background is neutron capture of ^{40}Ca: ^{40}Ca(n,γ)^{41}Ca [4].
New measurements will help to improve data on the terrestrial influx of extraterrestrial material. This can play an important role for various research fields, i.e. modelling the interplanetary dust cloud [5]. ^{41}Ca provides the chance for an approach, independent from yet established methods, to determine the influx of interplanetary dust.

This thesis is divided into three chapters. In the first chapter, the origin of interplanetary dust and why it approaches earth is summarized.
In chapter two, based on the results stated in chapter one, an estimation of the extraterrestrial ^{41}Ca-influx to earth is made.
In chapter three, the results of chapter two are used to estimate the ratio between extraterrestrial ^{41}Ca-atoms and overall (mainly terrestrial) ^{40}Ca-atoms present in Antarctic ice. With Accelerator-Mass-Spectrometry at the MLL in Garching, this quantity can be measured down to ~10^{-16}. Furthermore, it is discussed, whether the terrestrial background of ^{41}Ca in Antarctic ice is negligible, i.e. whether ^{41}Ca can be used as tracer for extraterrestrial matter.

1 Interplanetary Dust Particles (IDP) on earth

1.1 Origin of Interplanetary Dust - The zodiacal cloud

The zodiacal cloud is a dust cloud surrounding all the objects in our solar system [6]. Actually the interplanetary dust particles form the zodiacal cloud. It is fed by disruption processes of larger objects like comets or asteroids. Dust particles' trajectories in a solar orbit converge towards the sun. This is caused by the so called Poynting-Robertson-Effect, explained in detail in chapter 1.2.
Sources of extraterrestrial material on earth are believed to mainly lie in our solar system. Figure (1) shows possible sources which are discussed in detail in [1]. According to Kortenkamp and Dermott [6], a significantly high and maybe dominant percentage (5-25%) of the dust in this zodiacal cloud has its origin in the asteroid belt at 3AU from the sun (see figure (1)). 1 astronomical unit (AU) is the average distance between earth and sun $\left(1\,AU \approx 1.5 \cdot 10^{13} cm\right)$. Other Authors [7] even surpass the Kortenkamp and Dermott value of asteroidal contribution by stating 30-50%. Among asteroids, the other main source of interplanetary dust is comets [6], [7]. Details about origin and processes of the interplanetary dust cloud are not well characterized.

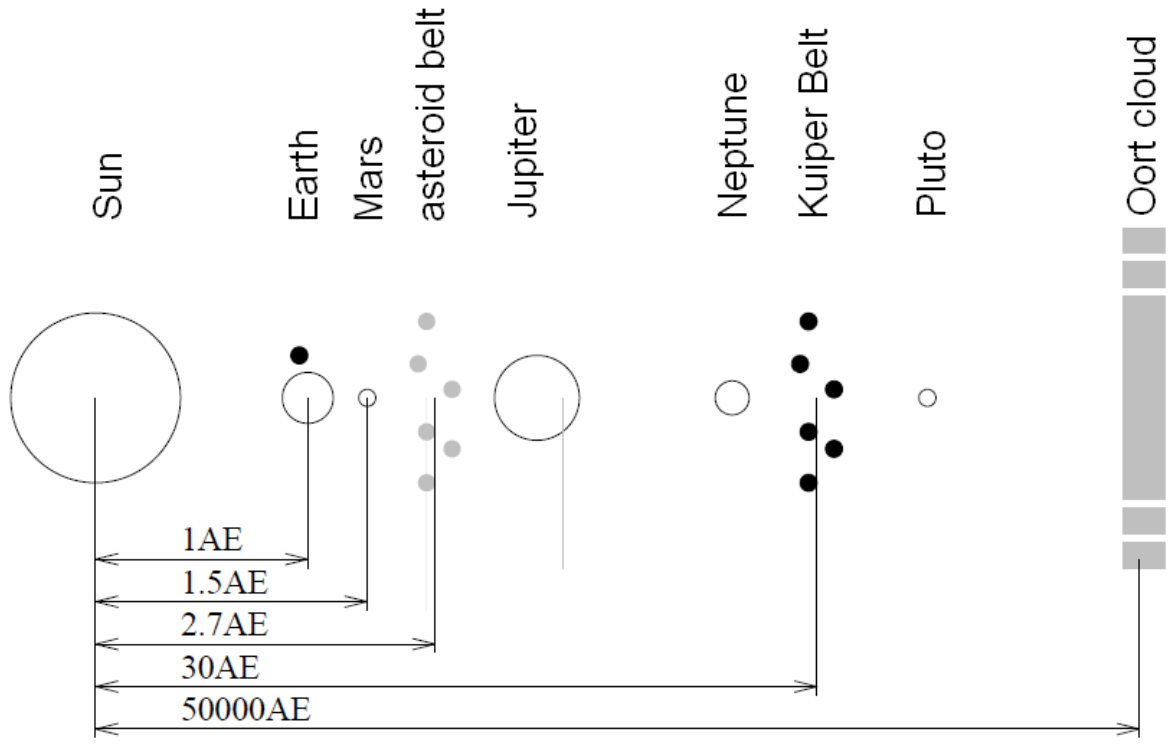

Figure (1): sketch of the solar system; in the original work AE is used for “astronomical unit” (AU in this work); taken from [1]

1.2 Motion of IDP

Forces acting on particles in our solar system are dominantly induced by the sun. Besides sun's gravitational force, for IDP also non-gravitational forces contribute significantly. Scattering of light and interaction with solar wind particles (mostly hydrogen-plasma) are the two forces which are included in the model described in chapter 2.3.

The scattering of solar light slows the particles down and lets their orbit decrease towards the sun. This so called the Poynting-Robertson-Effect will be explained in the following. “Scattering” of solar wind particles also forces IDP towards the sun. In fact, for describing the scattering of particles instead of photons, only the relation between energy and momentum needs to be adapted. A detailed derivation and further references on that topic can be found in [8].

1.2.1 Poynting-Robertson-Effect

Consider a particle with velocity $\vec{v} = v\vec{e}_z$ being irradiated perpendicular to $\vec{v}$ by incident light with Poynting-Vektor $\vec{S}$. Such a set-up is shown in figure (2b). This corresponds to a dust particle on a circular orbit around the sun described in the sun's rest frame. Using the Lorentz-transform, the situation can also be described in any other inertial frame. In the rest frame of the particle, the radiation $\vec{S}_{rest\ frame}$ is not perpendicular to the velocity $\vec{v}_{rest\ frame}$ (figure (2a)). Therefore, in this reference frame, there is a component of $\vec{S}_{rest\ frame}$ which is parallel to $\vec{v}_{rest\ frame}$. Consequently, absorbing a photon causes the z component of the velocity to change. Note that during the reaction the particle's momentum is changed which causes the rest frame to be an accelerated but not an inertial reference frame. In order to work with inertial reference frames only, “rest frame” is now defined as the reference frame where the particle is at rest after one photon is absorbed. In the original reference frame, where the radiation $\vec{S}$ is perpendicular to $\vec{v}$, the absorption of a photon does not change the velocity's z-component. However, when the particle is in thermal equilibrium, it needs to re-emit the energy it absorbs. In the rest frame, the emission is isotropic and thus, on average over many photon emissions, does not change the velocity $\vec{v}_{rest\ frame}$. In the original reference frame, the emission of light is anisotropic due to the (relativistic) Doppler effect. Photons emitted in forward direction carry more momentum than those emitted in backward direction. Consequently the particle becomes decelerated along the z-direction.
A detailed calculation by Burns et al. [8] delivers differential equations for eccentricity and semi-major axis for those particle's orbits.

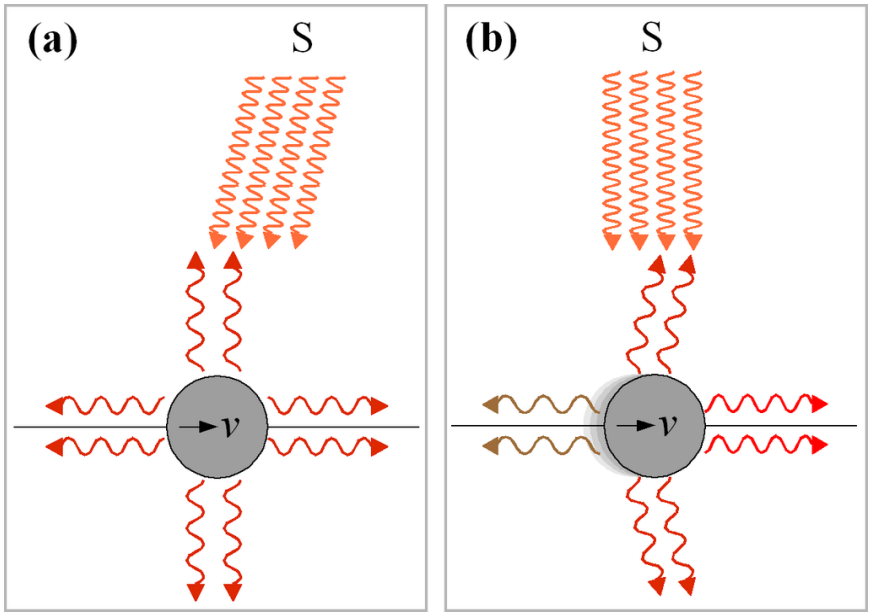

Figure (2): Poynting-Robertson-Effect in the rest frame of the particle (a) and in the rest frame of the irradition-source (b); Figure taken from [9]

1.3 Spallation-processes in IDP – cosmic rays

High energetic particle irradiation present at the top of earth's atmosphere is called (primary) cosmic rays. They are classified into a solar and a galactic component. The solar component originates from our sun and mainly consists of protons (>90%, [10], [1]). The galactic component is believed to originate from supernovae explosions and also mainly consists of protons (~87%, [10], [1]). The second most abundant component in cosmic rays are α-particles followed by less than 1% of heavier nuclei [10], [1], [11]. The solar and galactic cosmic rays vary periodically over the ~11yr long solar cycles [11]. Because interplanetary dust particles are exposed to cosmic rays for 10^4 years or even longer (see [2], [12], formula (8)), i.e. at least 3 orders of magnitude higher, the modulation effect on galactic cosmic rays (GCR) and variations in solar cosmic rays (SCR) are neglected. In this work, the average GCR proton flux measured in [13] will be used and assumed to be constant in every calculation (Appendix B). SCR flux-data are only used qualitatively. A plot of the average cosmic ray fluxes at 1AU (from the sun) is shown in figure (3).
In the following, whenever “at xAU” is written, it is meant in a distance of x AU from the sun.

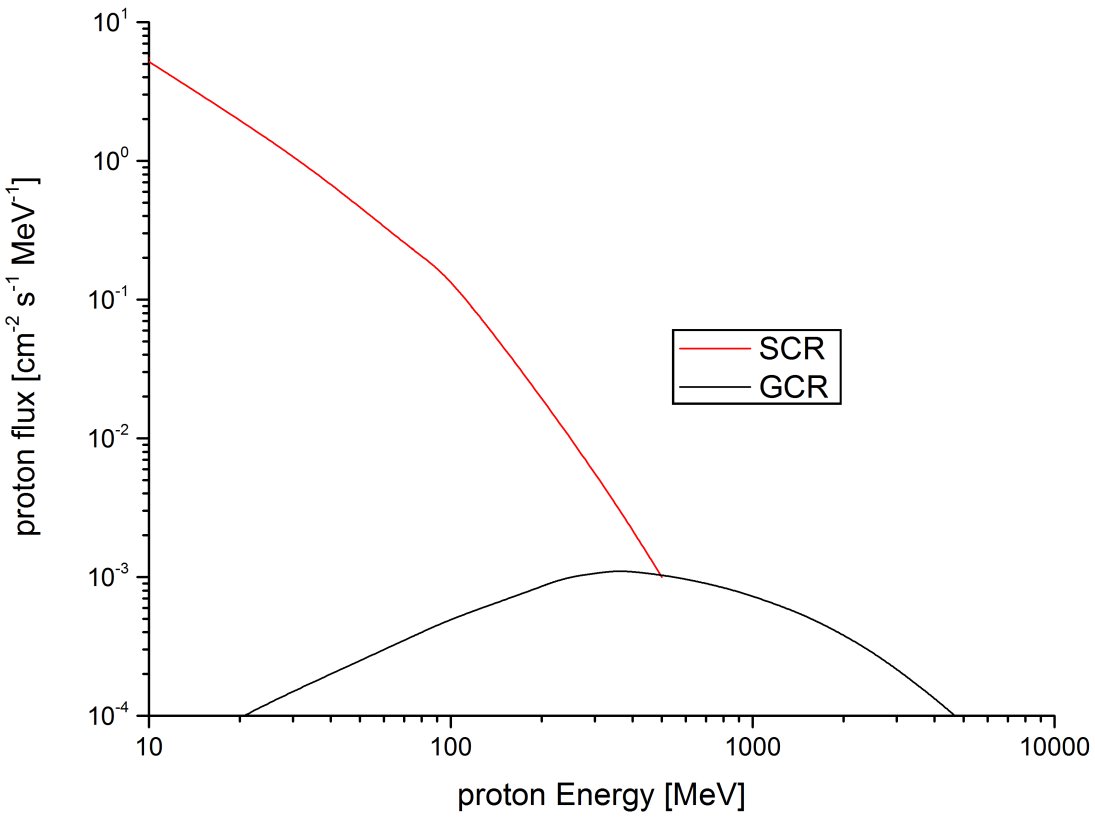

Figure (3): average proton flux distribution at 1AU (values taken from [10], [13])

Spallation means that a nucleus is divided into one or more nuclei because of a high energetic incident particle. For production of radionuclides in IDP, spallation processes like ^{56}Fe + p → ^{41}Ca + ”balance” play an important role. In chapter 2.2, this reaction is discussed to be the major source of ^{41}Ca in interplanetary dust.
For a reaction like “target” + “projectile” → “product” + ”balance” (in the following, the term + ”balance” will not be written any more, but implicitly it is needed to balance the equation), formula (1) defines the cross-section σ. Φ is the flux of incident particles (projectile,

these are the protons “p” in the example in the previous paragraph) $[\Phi]=\frac{particles}{cm^2\,s}$, N_{target} the number of atoms of the target material (^{56}Fe in the example in the previous paragraph). The reaction rate is the number of “product”-atoms produced per unit time. In the following, this will be called the production-rate and be named p. Φ can be divided into a solar and a galactic part, as discussed above $\left(\Phi=\Phi_S+\Phi_G\right)$. Whenever p is indexed with S or G, only production due to solar or only due to galactic projectiles is meant.

$$p\equiv\text{'reaction rate'}=\Phi\cdot\sigma\cdot N_{target} \tag{1}$$

When σ and Φ are energy-dependent, it has to be summed (integrated) over all energies. The result is formula (2), which states how the production-rate of a radionuclide p per number of target nuclei N_{target} is linked to spallation cross-section $\sigma(E)$ and proton-flux $\frac{d\,\Phi(E)}{dE}$.

$$\frac{p}{N_{target}}=\int\frac{d\,\Phi(E)}{dE}\cdot\sigma(E)\;dE \tag{2}$$

In the literature, values like $x\frac{dpm}{kg(target)}$ are often found (dpm = disintegrations per minute). A production-rate of $1\frac{dpm}{kg(target)}$ means, that in 1kg of target material within one minute one product-atom is produced. In this work, among $1\frac{dpm}{kg(target)}$, also $1\frac{dpm}{kg}$ will be used. A production-rate of $1\frac{dpm}{kg}$, means that in 1kg of sample material within one minute one product-atom is produced. So, the production-rate is normalized to target mass m and not to the number of target atoms N_{target}. This can be easily converted via the molar mass M of the target atom and Avogadro's constant N_A $N_{target}=\frac{m}{M}N_A$.

Conversion between $1\frac{dpm}{kg}$ and $1\frac{dpm}{kg(target)}$ depends on the abundance of target material in the sample. When the sample has x mass-% of target material, then $1\frac{dpm}{kg(target)}=x\,\%\cdot\frac{dpm}{kg}$.

Because normalization only changes values by a constant factor, it will not always be distinguished between $\frac{p}{N_{target}}$, $\frac{p}{m_{target}}$, $\frac{p}{m_{whole\ sample}}$, … When calculations are made, the production-rate will simply be named p, however it is normalized. From the context of its unit $\left(1\frac{dpm}{kg}\text{ or }1\frac{dpm}{kg(sample)}\right)$, the normalization used becomes unique and can be converted as stated above.

2 Accretion of ^{41}Ca from IDP on earth

The aim of this chapter is to estimate the accretion rate of extraterrestrial ^{41}Ca from interplanetary dust on earth. At first, it is shown that the most important reaction to produce ^{41}Ca in IDP is spallation of iron. Secondly, outgoing from measurements of extraterrestrial ^{53}Mn, an accretion rate of ^{41}Ca is derived. Finally, the accretion rate is estimated with a model independent from the ^{53}Mn-measurements. It is explained why these estimations represent a lower and an upper limit of accreted ^{41}Ca.

2.1 Sources of ^{41}Ca in IDP

There are two major reactions for the production of ^{41}Ca in IDP [4]: Spallation of iron and nickel due to cosmic proton irradiation and neutron capture of the most abundant stable Ca-isotope ^{40}Ca. In the following, it will be shown that neutron capture and spallation of nickel contribute only negligibly to the total abundance of ^{41}Ca in IDP compared to spallation of iron at 1AU. The results are summarized in figure (4).

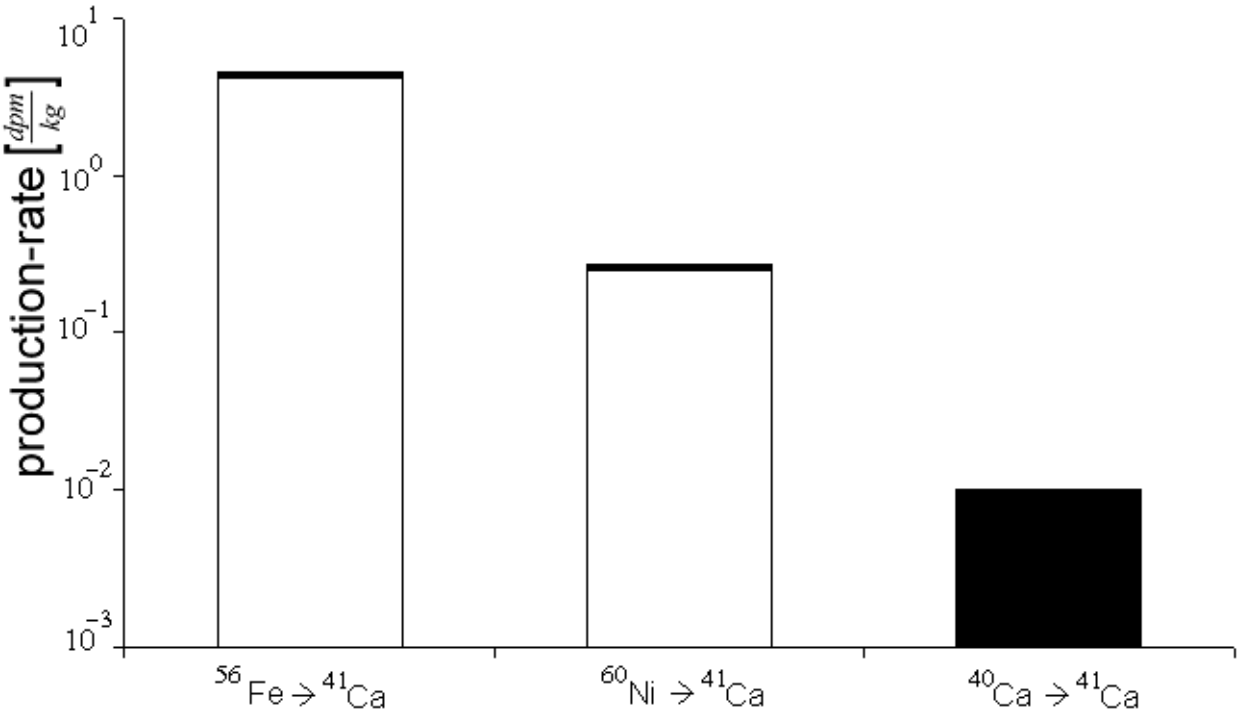

Figure (4): Production-rates of ^{41}Ca at 1AU via the different production channels spallation of nickel and iron among neutron capture of ^{40}Ca. Black marked areas denote uncertainties. For the reaction ^{40}Ca(n,γ)^{41}Ca only an upper limit is provided.

2.1.1 Spallation of iron and nickel due to cosmic rays

Spallation reactions, cross-sections and production-rates have been introduced in chapter 1.3. $\frac{d\,\Phi(E)}{dE}$ does not depend on the target material considered, i.e. is the same for the reactions ^{56}Fe + p → ^{41}Ca and ^{60}Ni + p → ^{41}Ca. The spallation cross-sections $\sigma(^{60}\text{Ni}\rightarrow^{41}\text{Ca})$ and $\sigma(^{56}\text{Fe}\rightarrow^{41}\text{Ca})$ are very similar (Appendix A, [14]). Therefore, the production rates mainly depend on the abundance of the target material N_{target} (formula (2)). Because IDP

contains about 17 times more (related to mass) iron than nickel (see Appendix C), the production due to spallation of iron is about 17 times higher than spallation of nickel.

At earth's orbit (1AU), the production rate due to spallation of iron is $p_{Fe\to Ca}=24\pm1\,\frac{dpm}{kg(Fe)}$, provided by different authors using independent methods [15], [16], [17]. With 18.2 weight-% iron in IDP (see Appendix C), the production-rate in IDP is $p_{Fe\to Ca}=4.37\pm0.19\,\frac{dpm}{kg}$.

Dividing by 17 provides the production-rate from nickel $p_{Ni\to Ca}=0.26\pm0.01\,\frac{dpm}{kg}$.

2.1.2 Neutron capture of ^{40}Ca

The production rate due to neutron capture in IDP at 1AU is smaller than 0.01 $\frac{dpm}{g(Ca)}$ [18] for particles with radii smaller than 10cm. In this work, only dust particles with much smaller radii are considered, because the contribution of bigger particles to the terrestrial accretion is negligible (see Appendix D). With about 1 weight-% of ^{40}Ca in IDP, this corresponds to $p_{^{40}Ca\to{}^{41}Ca}\le0.01\,\frac{dpm}{kg}$.

2.2 Upper limit estimation - Comparison between ^{53}Mn and ^{41}Ca

Among ^{41}Ca ($t_{½}$=1.03 x 10^5 yr; [19]), ^{53}Mn ($t_{½}$=3.68 x 10^6 yr; [19]) is another long lived radionuclide which can be used to trace interplanetary dust on earth. Like for ^{41}Ca, the most important source of extraterrestrial ^{53}Mn is known to be spallation of iron (>90%) [1]. However, the production cross-section for the spallation reaction ^{56}Fe+p→^{53}Mn starts to be significant at much lower proton energies (~1-10MeV, [14]) than for ^{41}Ca.

Let x_{Mn} be the fraction of ^{53}Mn and x_{Ca} the fraction of ^{41}Ca that is produced by spallation of iron at proton-energies between 180MeV and 1680MeV of only the galactic cosmic ray protons. [^{41}Ca] and [^{53}Mn] denote the concentration of ^{41}Ca and ^{53}Mn in IDP at 1AU. During the motion, ^{41}Ca and ^{53}Mn are produced, but at the they also decay according to their decay-constant. When decay is neglected, the ratio between [^{41}Ca] and [^{53}Mn] is equal to their production-rates (equation (3), also compare chapter 1.3).

$$\frac{x_{Ca}}{x_{Mn}}\cdot\frac{[^{41}Ca]}{[^{53}Mn]}=\frac{x_{Ca}}{x_{Mn}}\cdot\frac{p_{Ca}}{p_{Mn}}=\frac{\int_{180\mathrm{MeV}}^{1680\mathrm{MeV}}\frac{d\,\Phi(E)}{dE}\cdot\sigma_{Fe\to Ca}(E)\;dE}{\int_{180\mathrm{MeV}}^{1680\mathrm{MeV}}\frac{d\,\Phi(E)}{dE}\cdot\sigma_{Fe\to Mn}(E)\;dE} \qquad (3)$$

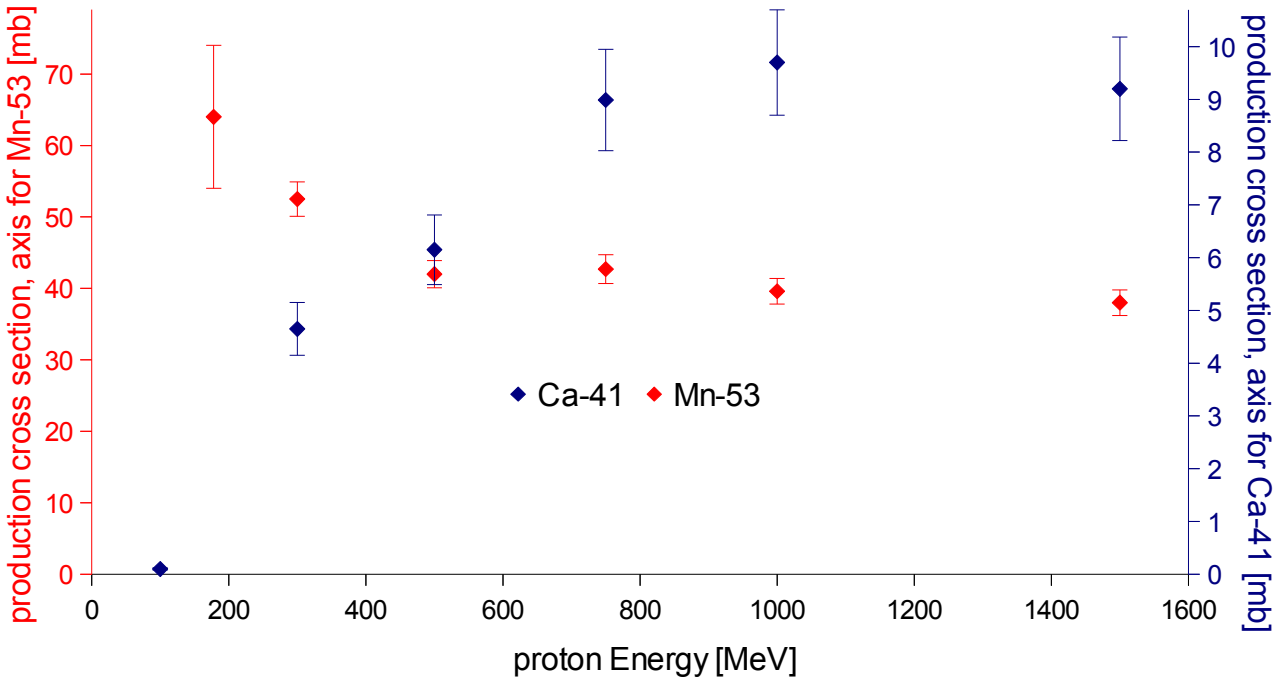

Figure (5): cross sections for spallation of iron to ^{41}Ca and ^{53}Mn (values taken from [20], [14], [21]); the left y-axis corresponds to ^{53}Mn, the right y-axis corresponds to ^{41}Ca

The integration is performed stepwise, because only data at discrete energies are available. The values in Appendix A and B yield to calculate the following:

$$\int_{300\mathrm{MeV}}^{1500\mathrm{MeV}} \frac{d\,\Phi(E)}{dE}\cdot\sigma(E)\;dE \approx \sum_{E}\sigma(E)\Phi(E)$$

to evaluate at E=
300MeV, 500MeV, 750MeV, 1000MeV, 1500MeV

The calculation states $\frac{x_{Ca}}{x_{Mn}}\cdot\frac{[^{41}Ca]}{[^{53}Mn]} \approx 0.18\pm0.01$.

x_{Ca} is bigger than x_{Mn} for the following reasons: The production cross-section for ^{53}Mn arises at energies lower than 180MeV, whereas the cross-section for the production of ^{41}Ca drops to <0.1mb for energies <100MeV ([14], figure (5)). In addition, the proton flux at energies <100MeV (dominated by the solar component) is several orders of magnitude higher than the total flux within the considered energy-range (figure (3), p. 6).

So, using $\frac{x_{Mn}}{x_{Ca}} < 1$, formula (4) holds:

$$\frac{[^{41}Ca]}{[^{53}Mn]} \approx \frac{x_{Mn}}{x_{Ca}}\cdot(0.18\pm0.01) < 0.19 \Rightarrow [^{41}Ca] < 0.19\,[^{53}Mn] \qquad (4)$$

This relation can also be used for the annual accretion-rates R of both radionuclides, when the accretion behaviour is assumed to be equal (formula (5)).

$$\frac{R(^{41}Ca)}{R(^{53}Mn)} = \frac{[^{41}Ca]}{[^{53}Mn]} < 0.19 \qquad (5)$$

Author(s)	year of publication	^{53}Mn accretion-rate $\left[10^3 \frac{at}{yr\ cm^2}\right]$	comment	Ref.
Bibron et al.	1974	18.4 ± 4.2	average global	[22]
Bibron et al.	1974	6.1 ± 1.4	at their sampling site	[22]
Imamura et al.	1979	1.954 ± 0.084	-	[23]

Table (1): Accretion-rates of ^{53}Mn by different authors

^{53}Mn-accretion rates provided by different authors are listed in table (1). Bibron et al. state an accretion-rate of $6.1 \pm 1.4 \cdot 10^3 \frac{at}{cm^2\ yr}$ at their sampling site near the Antarctic Plateau Station (79°15'S, 40°30'E). Then, they extrapolate their value to global average using a model that assumes an anisotropic accretion of aerosols. According to their model, the accretion-rate at the poles can be seen as lower limit. Because little is known about that topic, in this work, isotropic accretion on the whole surface of the earth is assumed as first approach. Their approach of extrapolation is mentioned for completion only. For further calculations, the accretion of IDP is assumed isotropic. So the upper limit for the accretion-rate of ^{53}Mn is set to $R(^{53}Mn) \leq 6.1 + 1.4 \cdot 10^3 \frac{at}{cm^2\ yr} \leq 7.5 \cdot 10^3 \frac{at}{cm^2\ yr}$, which is the value Bibron et al. measured in their samples. Then the upper limit for the accretion-rate of ^{41}Ca is (using formula (5)) $R(^{41}Ca) < 1.4 \cdot 10^3 \frac{at}{cm^2\ yr}$.

2.3 Lower limit estimation - Model of production-processes in IDP

To estimate the expected amount of ^{41}Ca in the IDP when accreted, among production rates and elemental composition, also the time being exposed to cosmic irradiation is important. A significant proportion of interplanetary Dust on earth is believed to originate the Asteroid Belt at about 3AU in our solar system (see chapter 1.1). Consequently, this model considers particles originating (i.e. being produced) from 3AU. In this chapter, all IDP is assumed to come from the Asteroid Belt. After production, IDP approaches earth due to the combined action of solar gravitation and Poynting-Robertson-Effect (see chapter 1.2). Other forces, for example interactions with Mars or collisions between dust particles, are not considered. This also means that changes in mass and size of IDP during the motion (for example because of collisions) do not occur in the model. Moreover, corrections due non circular but elliptical orbits are neglected. Furthermore, it is assumed that the particles have no ^{41}Ca-content when they are produced. Therefore the obtained values can be interpreted as a lower limit for the concentration of cosmogenic ^{41}Ca at 1AU. The only ^{41}Ca-producing reaction considered in this model is the spallation of iron induced by cosmic proton irradiation (^{56}Fe + p → ^{41}Ca). In chapter 2.1 is shown, that this is the major reaction for the formation of cosmogenic ^{41}Ca. This model has recently been used by Auer and seems to comply with measurements [12], [2].
Formula (6) denotes the decay law in combination with production of ^{41}Ca. N(t) is the number of ^{41}Ca atoms, λ the decay constant of ^{41}Ca ($\lambda = \frac{\ln(2)}{t_{1/2}}$, $t_{½}$=1.03 x 10^5 yr) and $p_{S,G}$ the production rate of ^{41}Ca induced by solar (SCR) and galactic (GCR) protons. p_G is assumed to be constant with time, while p_S has a time dependence (denoted in formula (9), explanation follows).

$$\frac{dN(t)}{dt} = -\lambda N(t) + p_S(t) + p_G \tag{6}$$

Formula (7) describes the motion of a particle with radius r and density ρ in a circular orbit around the Sun due to the Poynting-Robertson-Effect (see chapter 1.2 and equation (12) in [6]). a(t) is the distance of the dust particle from the Sun, S_0 $\left([S_0] = 1\frac{J}{m^2 s^2} = 1\frac{kg}{s^4} \right)$ the Sun's Luminosity per steradian and c the speed of light. In [8], formulas describing the motion of IDP on elliptical orbits are derived. In this work, only circular orbits (this means eccentricity is zero) are considered. So in the formulas in [8], the eccentricity is set to zero. In addition, [8] derives the formulas for particles that transmit, scatter and absorb a certain percentage of the incident light. These properties are coded into a quantity called "efficiency factor". For an isotropically scattering and non transmitting particle, the efficiency factor is 1, which is assumed for IDP. In chapter 1.2 it has been mentioned that particle irradiation has the same effect on IDP as light irradiation. It is assumed, that the force due to the emitted particles by the sun (the so called solar wind) is 30% [6] of the force by the Poynting-Robertson-Effect (factor 1.3 = solar light force + solar wind force = solar light force + 30% * solar light force = 1.3 * solar light force). In the following, a constant k is defined and used as $-1.3\frac{3S_0}{2c^2} = -1.3 \cdot 5.12 \cdot 10^{11}\frac{g}{s} \equiv k$. Putting all the mentioned facts and assumption together results in formula (7). A derivation and deeper explanation of the Poynting-Robertson-Effect can be found in [8].

The density of IDP is predicted to be ρ= 2.5 g cm^{-3} ([6], [8], [5], [2]).
Considering the boundary-condition $a(t=0) \equiv a_0 \equiv 3\,AU$, i.e. a particle starting its flight from the asteroid belt at 3AU, ($1\,AU \approx 1.5 \cdot 10^{13} cm$) the equation of motion (formula (7)) can be solved and resolved for the time of flight "t" (equation (8)).

$$\frac{da(t)}{dt} = \frac{k}{\rho r\, a(t)} \tag{7}$$

$$t = \left(a_0^2 - a(t)^2\right) \cdot \frac{\rho r}{2k} \tag{8}$$

Formula (9) states the production-rate of ^{41}Ca induced by solar cosmic proton irradiation in dependence of time. Assuming isotropic solar (proton) irradiation Φ (i.e. the sun has no preferred direction for its emission of light and its emission of particles), its intensity at the particle's position is proportional to the inverse of the squared distance a(t) between dust particle and sun ("a(t)$^{-2}$"). In addition, the irradiation-intensity is proportional the production-rate (see explanation in chapter 1.3, especially formula (1)).

$$\Phi \propto \frac{p_S(t)}{a^2(t)} \Rightarrow \frac{p_{S,\,1\mathrm{AU}}}{(1\mathrm{AU})^2} = \frac{p_S(t)}{a^2(t)} \Rightarrow p_S(t) = p_{S,\,1\mathrm{AU}} \left(\frac{1\mathrm{AU}}{a(t)}\right)^2 \tag{9}$$

Together with the Poynting-Robertson movement (equations (7) and (8)) this allows to rewrite differential equation (6).

$$\frac{dN(t)}{dt} = -\lambda N(t) + \frac{p_{S,1\mathrm{AU}} \cdot (1\mathrm{AU})^2}{a_0^2 + \frac{2ct}{\rho r}} + p_G \qquad (10)$$

Solving the differential equation in formula (10) from t=0 to the time of flight (equation (8)), one obtains the number of ^{41}Ca-atoms in dependence of the dust particle's radius r. This last step is calculated using the computer algebra system “Wolfram Mathematica” (see figure (6)).

$$ExpIntegralEi(x) = -\ principal\ value\left(\int_{-x}^{\infty} \frac{e^{-t}}{t}\,dt\right) \qquad (11)$$

```
In[1]:= DSolve[{y'[t] == -λ y[t] + P a^2/(b^2 + 2 c t/(ρ r)) + A, y[0] == 0}, y, t]

Out[1]= {{y → Function[{t}, (e^(-t λ - b^2 r λ ρ/(2 c)) (-2 A c e^(b^2 r λ ρ/(2 c)) + 2 A c e^(t λ + b^2 r λ ρ/(2 c)) - a^2 P r λ ρ ExpIntegralEi[b^2 r λ ρ/(2 c)] + a^2 P r λ ρ ExpIntegralEi[t λ + b^2 r λ ρ/(2 c)]))/(2 c λ)]}}

In[3]:= g[r_, t_] := 1/(2 c λ) e^(-t λ - b^2 r λ ρ/(2 c)) (-2 A c e^(b^2 r λ ρ/(2 c)) + 2 A c e^(t λ + b^2 r λ ρ/(2 c)) - a^2 P r λ ρ ExpIntegralEi[b^2 r λ ρ/(2 c)] + a^2 P r λ ρ ExpIntegralEi[t λ + b^2 r λ ρ/(2 c)])

In[4]:= tfinal[r_] := (b^2 - a^2) ρ r/(-2 * c)

In[5]:= f[r_] := g[r, tfinal[r]]

In[6]:= f[r]

Out[6]= (e^(-b^2 r λ ρ/(2 c) + (-a^2 + b^2) r λ ρ/(2 c)) (-2 A c e^(b^2 r λ ρ/(2 c)) + 2 A c e^(b^2 r λ ρ/(2 c) - (-a^2 + b^2) r λ ρ/(2 c)) - a^2 P r λ ρ ExpIntegralEi[b^2 r λ ρ/(2 c)] + a^2 P r λ ρ ExpIntegralEi[b^2 r λ ρ/(2 c) - (-a^2 + b^2) r λ ρ/(2 c)]))/(2 c λ)
```

Figure (6): Screenshot of Mathematica-file written to calculate N(r). Because of limitations in Mathematica, some of the variables are named differently in this picture. For instance, no function in Mathematica can be named “N”. By comparison between the first line in the picture and formula (10), the variables can be correlated. The second line is the solution of (10), which is defined as function of r and t in line 3. The next two commands define the function N(r) (in Mathematica named “f[r]”), whose analytical expression is written in the last line. ExpIntegralEi is defined in formula (11).

In the last line in figure (6), the formula for the expected number of ^{41}Ca-atoms N(r) per target material (^{56}Fe) in interplanetary dust particles with radius r at 1AU is written.
Out of N(r), earth's influx of extraterrestrial ^{41}Ca-atoms can be calculated. $df(r)$ is the percentage of the total influx of extraterrestrial mass $\left([df(r)] = \frac{1}{time}\right)$ between a specific particle-radius r and r+dr. Then $N(r) \cdot df(r) = N(r) \cdot \frac{df(r)}{dr} dr$ is the influx of atoms originating from IDP with radii between r and r+dr. To obtain the total influx R* of extraterrestrial ^{41}Ca-atoms it has to be integrated over all radii r (equation (12)). In [5] a mass distribution of accreted interplanetary dust is delivered and discussed in detail in Appendix D.

$$R^* = \int dr\, N(r) \cdot \frac{d\,f(r)}{dr} \qquad (12)$$

2.3.1 Applying the model

Although the explanation of the model is specifies it for ^{41}Ca, it can be easily adopted to every other radionuclide. In order to do that, only the decay constant λ, and the production rates $p_{G;S,1\mathrm{AU}}$ need to be modified.
For ^{41}Ca, the following values are found in the literature:

$t_{½}(^{41}Ca)=1.03 \times 10^{5}$ yr (see [19]) => $\lambda(^{41}Ca)=\frac{\ln(2)}{t_{1/2}(^{41}Ca)}\approx 6.73\cdot 10^{-6}\,yr^{-1}$

$p_G=5.93\pm 0.38\,\frac{dpm}{kg(Fe)}$ (calculated as denoted in the following paragraph)

$p_{S,1\mathrm{AU}}+p_G=24\pm 1\,\frac{dpm}{kg(Fe)}$ (see [15], [16], [17]) => $p_{S,1\mathrm{AU}}=18.1\pm 1.1\,\frac{dpm}{kg(Fe)}$

The total production-rate of ^{41}Ca has been measured to be $p_S+p_G=24\pm 1\,\frac{dpm}{kg(Fe)}$. Subtracting the galactic part p_G delivers the solar part $p_{S,1\mathrm{AU}}$. The galactic production rate p_G is estimated using spallation cross sections on iron (Appendix A) and galactic proton fluxes. Table (2) in Appendix A provides cross-sections for the reaction ^{56}Fe+p→^{41}Ca at five energies between 300MeV and 1500MeV. In table (4), Appendix B, galactic proton fluxes at these five energies are listed. Using formula (13), the above stated production-rate p_G can be calculated.

$$p_G=\sum_E \phi(E)\cdot\sigma(E) \qquad (13)$$

For conversion between $\frac{dpm}{kg(Fe)}$ and $\frac{dpm}{kg}$, IDP has been assumed to have CI chondritic composition (see Appendix C) i.e. to have 18.2mass-% ^{56}Fe, i.e. $1\,\frac{dpm}{kg(Fe)}=0.182\cdot\frac{dpm}{kg}$ (see chapter 1.3).
In order to perpetuate the lower limit estimations in this chapter, for $p_{S,G}$ and λ the lower limits have been put into the model calculation. N(r=d/2) as written in figure (6), can now be plotted (figure (7)). Note, that in fact the number of ^{41}Ca-atoms in dependence of the particle's diameter, not the radius is plotted.

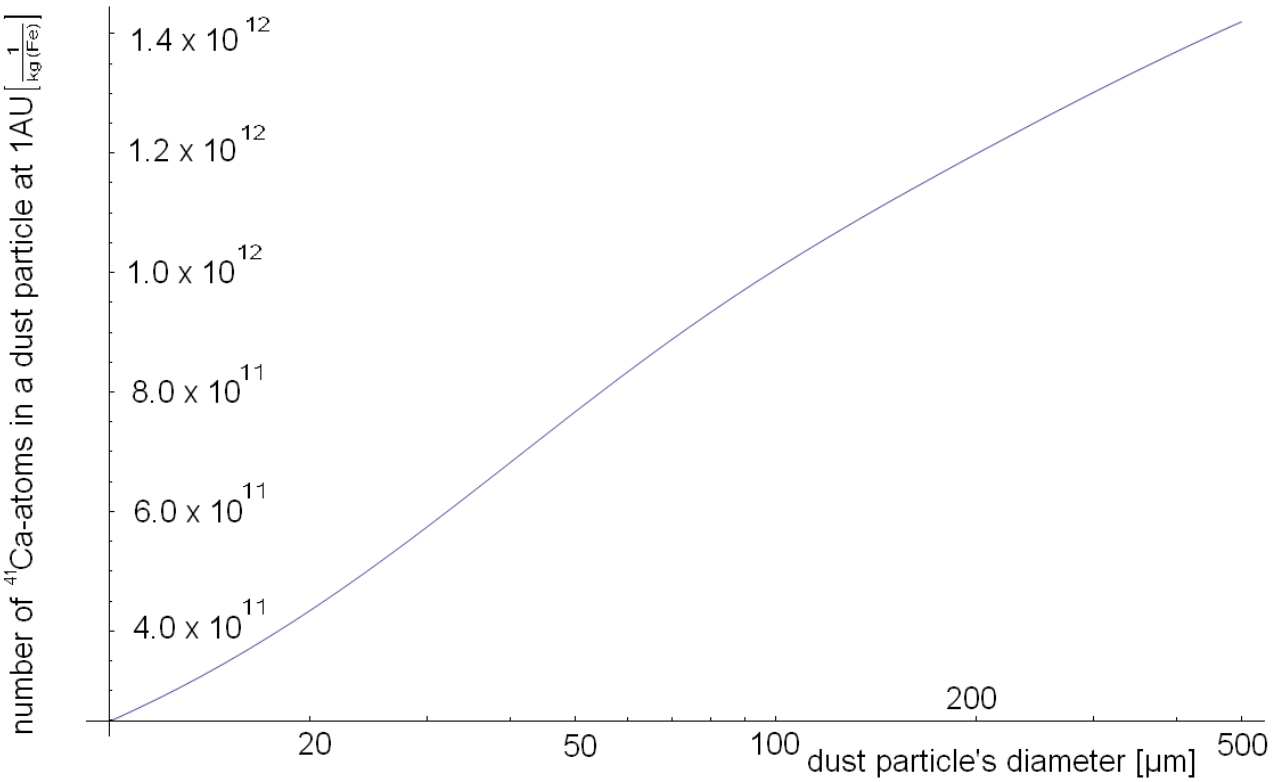

Figure (7): Number of ^{41}Ca-atoms N(d) in an interplanetary dust particle with diameter d after flying from 3AU to 1AU and with no ^{41}Ca-content at 3AU

Integration like denoted in formula (12) yields an accretion rate of $R^*(^{41}Ca)=6.14\cdot10^{18}\frac{at}{yr}$. Normalized to the earth's surface area (earth's radius is 6371km) the accretion-rate is $R(^{41}Ca)=\frac{R^*(^{41}Ca)}{\text{earth's surface area}}=1.20\frac{at}{yr\ cm^2}$.

2.4 Discussion

2.4.1 Upper limit

In the derivation (see chapter 2.2), it is assumed that the fraction x_{Mn} of spallation-produced ^{53}Mn at proton-energies between 180MeV and 1680MeV is smaller than the same fraction x_{Ca} for ^{41}Ca. In the calculation this is introduced by the statement $\frac{x_{Mn}}{x_{Ca}}<1$.

Most probably the ratio between x_{Mn} and x_{Ca} is much smaller than one: Comparing the flux of solar and galactic protons (figure (3)), it can easily be seen that the solar flux is between two and three orders of magnitude higher than the maximum of the galactic flux. Moreover, solar proton fluxes become negligible for energies higher than ~500MeV. The proton induced production cross-section for ^{53}Mn between 10 MeV and 10 GeV varies between 10mb and 200mb [14], i.e. is almost constant. The production of ^{53}Mn seems to be dominated by the solar protons due to the much higher solar flux at lower energies. For the production of ^{41}Ca, most of the solar protons have not enough energy (σ(E<100MeV) < 0.1mb). Its contribution to produce ^{41}Ca is probably subordinated. This means that for ^{41}Ca, the most important proton-energies are within the considered range (180MeV - 1680MeV), whereas for the production of ^{53}Mn the probably most important energies (solar cosmic rays) have been neglected. This statement is equivalent to “the ratio between x_{Mn}

and x_{Ca} is most probably much smaller than one“. However, the solar proton flux decreases with the squared distance from the sun (formula (9), p. 12). For a dust particle at 3AU, the production-rate due to solar protons reduces by a factor of 9.
Another uncertainty arises because the decay of ^{41}Ca and ^{53}Mn during their flight has been neglected completely.
In conclusion, the upper limit has a large uncertainty of two or three orders of magnitude.

2.4.2 Lower limit

In the model described in chapter 2.3, it has been assumed, that all the IDP is produced in the Asteroid Belt at 3AU and has no ^{41}Ca when produced. A different approach is to assume the equilibrium concentration. Including a concentration N_{3AU} results in an additive term: $N_{1AU,new} = N_{1AU,old} + N_{3AU} \times \exp(-\lambda t)$. The time of flight can be calculated via formula (8). The equilibrium-concentration at 3AU is $N_{3AU} = \left(p_G + p_{S,1AU} \cdot \frac{1\mathrm{AU}}{3\mathrm{AU}} \right) \cdot \lambda^{-1} = (9.35 \pm 0.58) \cdot 10^{12} \frac{at}{kg(Fe)}$. The shortest time of flight (10µm-particle) is about 53 x 10^3 yr which is about half the half-life of ^{41}Ca (compare formula (8)). For a 200µm-particle (maximum of terrestrial influx, see Appendix D) the time of flight is about one half-life (1.03 x 10^5 yr). So for a 10µm-particle assuming the equilibrium concentration at 3AU would mean two orders of magnitude more ^{41}Ca at 1AU (compare with figure (7)). For a 200µm-particle, introducing preliminary ^{41}Ca means a factor between 3 and 4 more ^{41}Ca at 1AU. Because the maximum terrestrial influx of IDP is at 200µm (see Appendix D), assuming no ^{41}Ca at 3AU is likely to produce an uncertainty of a factor less than 10.
Uncertainties because of non-circular orbits can be neglected. IDP originating from the Asteroid belt can be assumed to be on approximately circular orbits when produced. Moreover, according to calculations by Burns et al. [8], formula (14) holds for the eccentricity e. $\frac{de}{dt}$ is always negative which means all particles are forced towards having e=0, i.e. circular orbits. In conclusion, a particle starting with approximately circular orbit will stay on approximately circular orbits.

$$\frac{de}{dt} \propto -\frac{e}{\sqrt{1-e^2}} \quad \text{with positive proportionalyty-constant} \qquad (14)$$

In the model, cometary contribution to IDP is assumed to also originate from the Asteroid Belt. The uncertainty arising by this assumption is difficult to quantify. However, the cometary dust might only contribute negligibly to the accretion of IDP on earth [6].
Overall, the uncertainty of the lower limit is about a factor of 10.

2.4.3 Conclusion

The extraterrestrial influx of ^{41}Ca can lie between $1 \frac{at}{cm^2\,yr}$ and $10^3 \frac{at}{cm^2\,yr}$. The most probable influx lies near the lower limit, because the uncertainty of the upper limit much higher than for the lower limit.

3 ^{41}Ca as tracer for interplanetary dust in Antarctic snow?

3.1 Extraterrestrial ^{41}Ca in Antarctic snow

$\frac{[^{41}Ca]}{[^{all}Ca]}$ is an important quantity to be measured in Accelerator Mass Spectrometry [24]. With the conclusion from the previous page, an estimation of the atomic ratio $\frac{[^{41}Ca_{extraterr.}]}{[^{all}Ca]}$ in Antarctic ice can be made. In addition to the extraterrestrial influx of ^{41}Ca, the deposition-rate R(^{all}Ca) at the sampling site needs to be known. Calculations show that particles with radii smaller than 4µm have falling times in the time scale of less than 100 days [1] when only gravitation and stokes-friction are taken into account. Compared to the typical times of flight (see equation (8)) between 10^4 and 10^6 years, production of radionuclides during the time between entering the atmosphere and accretion can be neglected. In freshly deposited samples, the atomic ratio is equal to the deposition-rates (see equation (15)).

$$\frac{[^{41}Ca_{extraterr.}]}{[^{all}Ca]} = \frac{R_{extraterr.}(^{41}Ca)}{R(^{all}Ca)} \tag{15}$$

3.1.1 [^{41}Ca$_{extraterr.}$]/[^{all}Ca] at sampling site 73°6.378'S, 165°27.785'E

In [25], a deposition rate of $r(Ca) = 22 \pm 40 \frac{ng}{cm^2\, yr}$ has been determined at 73°6.378'S, 165°27.785'E, near Antarctica's coast. Using the average molar mass of calcium $M(Ca) = 40.08 \frac{g}{mol}$ [26] and Avogadro's Constant $N_A = 6.022 \cdot 10^{23} \frac{1}{mol}$ [26], the deposition-rate of ^{all}Ca can be calculated:

$R(^{all}Ca) = \frac{r(Ca)}{M(Ca)} \cdot N_A < 9.32 \cdot 10^{14} \frac{at}{cm^2\, yr}$ for $r(Ca) = 62 \frac{ng}{cm^2\, yr}$ as upper limit

$R(^{all}Ca) = \frac{r(Ca)}{M(Ca)} \cdot N_A = 3.31 \cdot 10^{14} \frac{at}{cm^2\, yr}$ for $r(Ca) = 22 \frac{ng}{cm^2\, yr}$ as average

So the lowest possible value for $\frac{[^{41}Ca_{extraterr.}]}{[^{all}Ca]} = \frac{R_{extraterr.}(^{41}Ca)}{R(^{all}Ca)}$ is $\frac{1.2}{9.32 \cdot 10^{14}} = 1.3 \cdot 10^{-15}$.

Now, the most probable ratio is going to be obtained. In the previous chapter it is discussed, why the lower accretion-rate of extraterrestrial ^{41}Ca is most suitable. So for the extraterrestrial still $R_{extraterr.}(^{41}Ca) = 1.2 \frac{at}{cm^2\, yr}$ is used, but $r(Ca) = 22 \frac{ng}{cm^2\, yr}$.

Thus the most probable value for $\frac{[^{41}Ca_{extraterr.}]}{[^{all}Ca]} = \frac{R_{extraterr.}(^{41}Ca)}{R(^{all}Ca)}$ is $\frac{1.2}{3.31 \cdot 10^{14}} = 3.6 \cdot 10^{-15}$.

Using the upper limit for $R_{extraterr.}(^{41}Ca)=1.4\cdot10^{3}\frac{at}{cm^{2}\,yr}$, the upper limit of the ratio is calculated as $\frac{1.4\cdot10^{3}}{3.31\cdot10^{14}}=4.22\cdot10^{-12}$, provided that $r(Ca)=22\frac{ng}{cm^{2}\,yr}$ is the lower limitation for the deposition-rate.
The AMS set-up at the Maier-Leibnitz Laboratory (MLL) in Garching is capable to measure a ratio of $\frac{[^{41}Ca]}{[^{all}Ca]}$ down to 10^{-16}. So, even in the case of the lower limit, the radionuclide could be detected at the specified sampling site.
Note, that $\frac{[^{41}Ca]}{[^{all}Ca]}$ varies with $\frac{1}{r(Ca)}$, i.e. strongly depends on the selected sampling site. Selecting a sampling site with small influx of ^{all}Ca (low r(Ca)) results in higher extraterrestrial contribution to the measurable quantity $\frac{[^{41}Ca]}{[^{all}Ca]}$.

3.2 Terrestrial ^{41}Ca in Antarctic snow

3.2.1 Equilibrium ratio [$^{41}Ca_{terr.}$]/[^{all}Ca]

Besides extraterrestrial produced ^{41}Ca, also terrestrial produced exists in the snow. At earth's surface, the production of ^{41}Ca is mainly cause by thermal neutron capture $^{40}Ca+n_{therm}\rightarrow{}^{41}Ca$ [4]. The cross-section for this reaction is $\sigma=0.41\pm0.02\,b$ [4] and the average neutron flux at Antarctica (to be precise, at geomagnetic latitude 50°) is $\phi\approx10^{-2}\frac{1}{cm^{2}\,s}$ [27]. So the equilibrium ratio can be calculated by adapting formula (6) to formula (16).

$$0\overset{!}{=}\frac{d[^{41}Ca_{terr.,eq.}](t)}{dt}=-\lambda[^{41}Ca](t)+\phi[^{40}Ca]\sigma\Rightarrow\frac{[^{41}Ca_{terr.,eq.}]}{[^{40}Ca]}=\frac{\phi\,\sigma}{\lambda}\qquad(16)$$

In numbers, the equilibrium terrestrial ratio is $\frac{[^{41}Ca_{terr.,eq.}]}{[^{40}Ca]}=(1.9\pm0.1)\cdot10^{-14}$ in Antarctica. Obviously, the terrestrial background cannot be neglected in general (compare with the extraterrestrial ratio obtained in previous chapter).

3.2.2 Origin of terrestrial Ca

The origin of accreted terrestrial calcium in Antarctica needs to be further researched. Therefore, no appropriate model for estimating the concentration of accreted [$^{41}Ca_{terr.}$] can be provided in this work. However, when material is freshly deposited, it is usually not in equilibrium with the environment. Rather than at the sampling site, the equilibrium at the origin of the terrestrial Ca should be considered. Considering the equilibrium at the terrestrial origin may still not be an appropriate approach, for example when exhumation goes faster than the time needed to reach equilibrium. The main production of terrestrial ^{41}Ca is induced by neutron-capture of the stable ^{40}Ca [$^{40}Ca(n,\gamma)^{41}Ca$] [4]. The neutron flux

reduces by a factor of ten every 3 meters [4]. So, where high erosion rates occur, the irradiation time may be too short to reach equilibrium at the surface.
Examination of terrestrial transportation processes is not this work's purpose, so no detailed discussion on that topic is included. Nevertheless, for tracing interplanetary dust with ^{41}Ca the origin of terrestrial ^{41}Ca definitely needs to be considered. In addition such a model would massively depend on the sampling site, so a general modelling is not sensible.

3.3 Conclusion

For tracing interplanetary dust by ^{41}Ca, the sampling site needs to be chosen very carefully. It has been shown, that the terrestrial background cannot be simply neglected (see chapter 3.2.1). Moreover, the origin of terrestrial incoming material has to be examined in order to estimate the terrestrial contribution to [^{41}Ca]. However, in principle it should be possible to trace IDP by ^{41}Ca, when the terrestrial deposition of ^{all}Ca is small enough. Different sampling sites should preliminarily be examined for the ^{all}Ca influx. When the extraterrestrial material is accreted isotropically on the whole planet, lower ^{all}Ca influxes corresponds to higher proportions of extraterrestrial ^{41}Ca influx.

Appendix

A Spallation cross-sections

A.1 $^{56}Fe+p\rightarrow^{41}Ca$ and $^{56}Fe+p\rightarrow^{53}Mn$

Table (2) lists the cross-section for the spallation reactions $^{56}Fe+p\rightarrow^{41}Ca$ and $^{56}Fe+p\rightarrow^{53}Mn$. These values are plotted in Figure (5).

E [MeV]	$\sigma_{Fe\rightarrow Ca}$ [mb]	E [MeV]	$\sigma_{Fe\rightarrow Mn}$ [mb]
1500	9.20 +- 0.98	1500	38.0 +- 1.8
1000	9.70 +- 1.00	1000	39.6 +- 1.8
750	8.99 +- 0.96	750	42.7 +- 2.0
500	6.15 +- 0.66	500	42.0 +- 1.9
300	4.65 +- 0.50	300	52.5 +- 2.4
100	0.10 +- 0.02	178	64 +- 10

Table (2) spallation cross-sections (values taken from [20], [14], [21])

A.2 $^{60}Ni+p\rightarrow^{41}Ca$

Table (3) lists the cross-section for the spallation reactions $^{60}Ni+p\rightarrow^{41}Ca$.

E [MeV]	$\sigma_{Ni\rightarrow Ca}$ [mb]	E [MeV]	$\sigma_{Ni\rightarrow Ca}$ [mb]
1600	9.5 +- 0.68	194	1.00 +- 0.29
1200	9.57 +- 0.67	188	0.39 +- 0.07
800	8.08 +- 0.80	172	0.58 +- 0.07
600	9.50 +- 0.90	148	0.16 +- 0.02
373	3.72 +- 0.16	140	0.31 +- 0.09
299	2.48 +- 0.21	98	0.09 +- 0.04

Table (3) spallation cross-sections (values taken from [28])

B Proton flux in cosmic rays

In Table (4), the galactic proton flux distribution used for calculations is listed. In [13], a differential proton-flux distribution at the top of earth's atmosphere is provided. These values are measured in between solar minimum and maximum, so the given spectrum should represent an overall time average. For calculating production rates as described in chapter 2.3, it is necessary to have absolute (say “integrated”) proton fluxes. The integration is carried out stepwise for the given intervals. Furthermore, the flux distribution needs to be adapted to the energies, where spallation cross-sections are available. For example, all protons with energies between 0.18 and 0.5 GeV are accredited to 0.3 MeV. Brackets “>” indicate the energy-ranges which are combined (summed).

differential spectrum				integrated spectrum			
E [GeV]		flux [m^{-2} s^{-1} sr^{-1} GeV^{-1}]			E [MeV]	Flux [cm^{-2} s^{-1}]	
0.18 – 0.20		651	+-	144			
0.20 – 0.23		715	+-	132			
0.23 – 0.27		801	+-	115			
0.27 – 0.33		845	+-	90	300	0.23	+- 0.01
0.33 – 0.40		892	+-	74			
0.40 – 0.50		848	+-	62			
0.5	- 0.63	793	+-	56	500	0.24	+- 0.01
0.63	- 0.8	715	+-	50	750	0.15	+- 0.01
0.80 – 1.02		622	+-	42	1000	0.36	+- 0.02
1.02 – 1.31		519	+-	36			
1.31	- 1.68	425	+-	29	1500	0.2	+- 0.01

Table (4): differential and integrated GCR proton flux distribution (differential values taken from [13]). The flux data is combined as indicated by brackets “>” for use with the provided spallation cross-sections in Table (2). Further explanation in the text.

C Average composition of interplanetary dust

The composition of interplanetary dust particles is similar to those of CI [29] or CM [30] chondrites, which are listed in table (4). In this work, IDP are assumed to have CI chondritic composition. As shown in chapter 2.1, the majority of extraterrestrial ^{41}Ca originates from spallation of iron. So, assuming CI chondritic IDP in chapter 2.3 means performing a lower limit estimation.

	CI	CM
O	46.0%	43.2%
Fe	18.2%	21.0%
Si	10.5%	12.9%
Ni	1.07%	1.20%
Ca	0.92%	1.27%
other	24.2%	21.7%

Table (4) mean composition of CM and CI chondrites; abundance of elements in mass-% (values taken from [31])

D Mass and size of accreted IDP

Reference [5] provides a graphical distribution of IDP accreted on earth in dependence of particles' size. In chapter 2.3, a calculation which needs a tabular distribution is presented. Unfortunately, no tabularized distribution could be found. So, a method to read the diagram every µm in between 10 and 500 µm needs to be found. One possibility is to find a fit function to the diagram. Such a function is written as formula (17). Thereby, f is the particle influx and m(d) the mass in dependence of the dust particle's diameter d. In this work, all particles are assumed to be spherical with density ρ, so mass and radius are connected

via formula (18). One possibility to check its quality is to plot it in the same diagram as the original plot. This has been done in figure (8).

$$\frac{d f(d)}{d \log\left(\frac{m(d)}{g}\right)} = \frac{16.25}{0.4} \cdot \frac{\exp\left[-\frac{1}{\left(-\frac{\log(d/\mu m)}{\log(500)-0.4}+\frac{4.5}{\log(500)-0.4}\right)^{8}}\right]}{\left(-\frac{\log(d/\mu m)}{\log(500)-0.4}+\frac{4.5}{\log(500)-0.4}\right)^{11.4}} \cdot 10^{-6}\,\frac{kg}{yr} \qquad (17)$$

$$m(d) = \frac{4}{3}\left(\frac{d}{2}\right)^{3}\pi\rho \qquad (18)$$

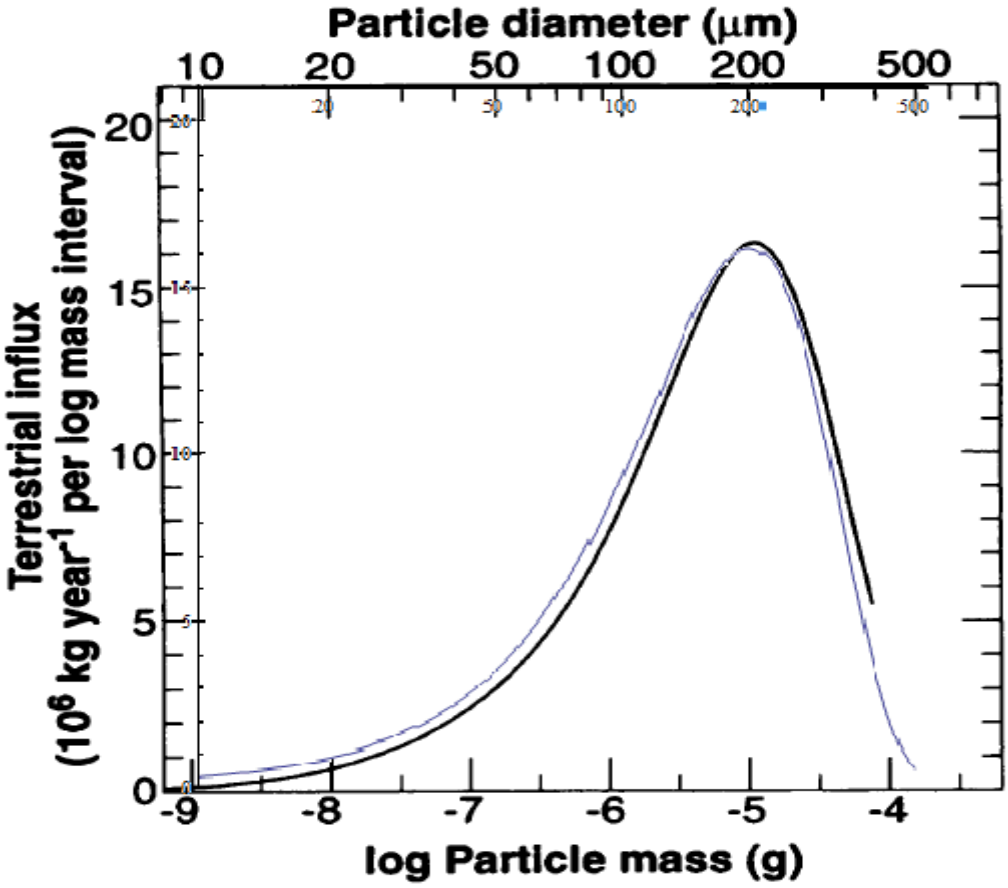

Figure (8): This image is originally taken from [5] and slightly modified.
Black curve: Mass distribution from Love and Brownlee [5]
Blue curve: Plotted function denoted in formula (17)

The fit-function is too high for IDP diameters smaller than ~200µm and too low for bigger particles. To summarize, the influx spectrum yielded by the fit is slightly shifted to smaller particles. The highest discrepancy of up to $2\frac{kg}{yr}\frac{10^{-6}}{\log(m)}$ occurs for $d \approx 200\mu m$. From d=400µm to d=500µm, no data is given in the diagram. In this range, the values of the fit-

function cannot be checked. For other diameters (i.e. smaller than 200μm) the discrepancy is $\leqslant 1 \frac{kg}{yr} \frac{10^{-6}}{\log(m)}$.

In addition to the diagram, Love and Brownlee also state "[i]ntegration of the mass distribution […] yields a total accretion rate of $40 \pm 20 \times 10^6 \frac{kg}{yr}$" [5]. Rewriting formula (17) only in terms of the mass m using formula (18), allows to integrate the fit-function from m(d=10μm) to m(d=500μm) over d(log(m(d)/g). The fit-function delivers a total mass influx of $\int_{10\mu m}^{500\mu m} \frac{d f(d)}{d \log\left(\frac{m(d)}{g}\right)} \cdot d \log\left(\frac{m(d)}{g}\right) = 31 \times 10^6 \frac{kg}{yr}$. So, the total influx is the same, within the uncertainty.

Bibliography

[1]: Tobias Schätz; 53Mn in extraterrestrischer Materie; Diploma Thesis, Technische Universität München E12, 1997

[2]: R. M. Auer et al.; Accretion rate of extraterrestrial 53Mn determined from aerosol and surface snow samples; Universität Wien, unpublished

[3]: Jozef Masarik, Robert C. Reedy; Terrestrial cosmogenic-nuclide production systematics calculated from numerical simulations; Earth and Planetary Science Letters 136, p. 381-395, 1995

[4]: D. Fink et al.; 41Ca: past, present, future; Nuclear Instruments and Methods in Physics Research B 52, p. 572-582, 1990

[5]: S. G. Love and D. E. Brownlee; A Direct Measurement of the Terrestrial MassAccretion Rate of Cosmic Dust; Science 262, p. 550-553, 1993

[6]: S. J. Kortenkamp, S. F. Dermott; Accretion of Interplanetary Dust Particles by the Earth; Icarus 135, p. 469-495, 1998

[7]: Sergei I. Ipatov; Dynamical zodiacal cloud models constrained by high resolution spectroscopy of the zodiacal light; Icarus 194, p. 769-788, 2008

[8]: J. A. Burns et al.; Radiation Forces on Small Particles in the Solar System; Icarus 40, p. 1-48, 1979

[9]: Poynting-Robertson-Effect; Wikipedia, July/12 2012; http://en.wikipedia.org/wiki/Poynting-Robertson_effect

[10]: R. Michel et al.; Simulation and modelling of the interaction of galactic protons with stony meteoroids; Planet. Space Sci. 43, p. 557-512, 1995

[11]: Astrid Meier; Messung von in situ produziertem 53Mn mit Beschleunigermassenspektrometrie; Diploma Thesis, Technische Universität München E15, 2006

[12]: R.M. Auer; Applications of 26Al in Atmospheric Research; Ph.D. Thesis, Universität Wien, 2008

[13]: W. Menn, M. Hof et al.; The absolute flux of protons and helium at the top of the atmosphere using IMAX; The Astrophysical Journal 533, p. 281-297, 2000

[14]: R. C. Reedy; Proton Cross Sections for producing cosmognic radionuclides; Lunar and Planetary Science Conference 38, p. 1192, 2007

[15]: Kuni Nishiizumi et al.; Depth profile of 41Ca in an Apollo 15 drill core and the low-energy neutron flux in the Moon; Earth and Planetary Science Letters 148, p. 545-552, 1997

[16]: J. Klein et al.; 41Ca in the Jilin (H5) Chondrite: A Matter of Size; Abstracts for the Annual Meeting of the Meteoritical Society 54, p. 120, 1991

[17]: D. Fink et al.; 41Ca in iron falls, Grant and Estherville: production rates and related exposure age calculations; Earth and Planetary Science Letters 107, p. 115-128, 1991

[18]: K. C. Welten et al.; Cosmogenic 41Ca in diognites: Production rates, pre-atmospheric size an terrestrial ages; Nuclear Instruments and Methods in Physics Research B 259, p. 653-662, 2007

[19]: J. Magill, G. Pfennig, J. Galy; Chart of the Nuclides; Marktdienste Haberbeck GmbH, Lage, Germany, 7th edition, 2006; ISBN: 92-79-02175-3

[20]: C. Villagrasa-Canton, A. Boudard, et al.; Spallation residues in the reaction 56Fe+ p at 0.3A, 0.5A, 0.75A, 1.0A, and 1.5A GeV; Physical Review C 75, p. 044603, 2007

[21]: S. Merchel et al.; Thin- and thick-target cross sections for the production of 53Mn and 60Fe; Nuclear Instruments and Methods in Physics Research B 172, p. 806-811, 2000

[22]: R. Bibron et al.; Extraterrestrial 53Mn in Antarctic ice; Earth and Planetary Science Letters 21, p. 109-116, 1974

[23]: M. Imamura et al.; 53Mn in deep-sea sediment cores - an indicator of past solar activity; International Cosmic Ray Conference 16, Vol. 2, p. 304-307, 1979

[24]: Klaus Knie; Beschleunigermassenspektrometrie mit Isobarenseparation in einem dedizierten gasgefüllten Magneten; Ph.D. Thesis, Technische Universität München, E15, 1997

[25]: Grazi a Ghermandi; Elemental and mineral characterisation of Coastal AntarcticAerosols in snow using PIXE and SEM-EDAX; Nuclear Instruments and Methods in Physics Research B 150, p. 392-397, 1999

[26]: Anton Hammer, Hildegard Hammer, Karl Hammer; Physikalische Formeln und Tabellen; J. Lindauer Verlag (Schaefer), München, Germany, 8. Auflage, 2005; ISBN: 3-87488-182-2

[27]: I. J. Graham et al.; Validation of cosmogenic nuclide production rate scaling factors through direct measurement; Nuclear Instruments and Methods in Physics Research B 172, p. 802-805, 2000

[28]: C. Schnabel et al.; Proton-induced production cross-sections and production rates of 41Ca from Ni; Nuclear Instruments and Methods in Physics Research B 223–224, p. 812–816, 2004

[29]: L. S. Schramm et al.; Major element composition of stratospheric micrometeorites; Meteoritics 24, p. 99-112, 1989

[30]: D. E. Brownlee; The elemental composition of stony cosmic spherules; Meteoritics and Planetary Science 32, p. 157-175, 1997

[31]: J. T. Wasson, G. W. Kallemeyn; Composition of chondrites; Philosophical Transactions of the Royal Society of London A 325, p. 535-544, 1988

Acknowledgements

I would like to thank the following people, who made it possible to finish this Thesis:

- Prof. Walter Henning for offering and supervising this work.
- Dr. Gunther Korschinek, Dr. Thomas Faestermann and Dr. José Manuel Gómez Guzmán for their assistance throughout my work.
- Leticia Fimiani, Peter Ludwig and Karin Hain for always answering my endless chain of questions.
- Andrew W. Strong (Max-Planck-Institut für extraterrestrische Physik) for the explanation of his database about cosmic ray fluxes.
- Valentina Chernenko, Clemens Herlitzius and the whole GAMS-group for providing a very pleasant working atmosphere.
- My family for supporting me all my life.